In the format provided by the authors and unedited.

Deglacial upwelling, productivity and CO$_2$ outgassing in the North Pacific Ocean

William R. Gray [1,2]*, James W. B. Rae [2], Robert C. J. Wills [3], Amelia E. Shevenell [4,5], Ben Taylor[2], Andrea Burke [2], Gavin L. Foster[6] and Caroline H. Lear[7]

[1]Department of Geography, University College London, London, UK. [2]School of Earth and Environmental Sciences, University of St Andrews, St Andrews, UK. [3]Department of Atmospheric Sciences, University of Washington, Seattle, WA, USA. [4]Department of Earth Sciences, University College London, London, UK. [5]College of Marine Science, University of South Florida, St Petersberg, FL, USA. [6]Ocean and Earth Science, University of Southampton, National Oceanography Centre Southampton, Southampton, UK. [7]School of Earth and Ocean Sciences, Cardiff University, Cardiff, UK. *e-mail: wrg4@st-andrews.ac.uk

# Deglacial upwelling, productivity and CO₂ outgassing in the North Pacific Ocean
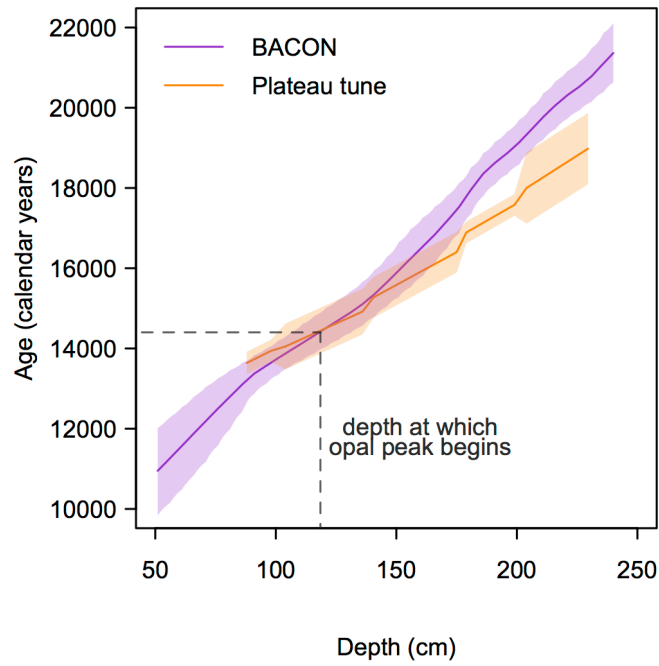
Supplementary Information
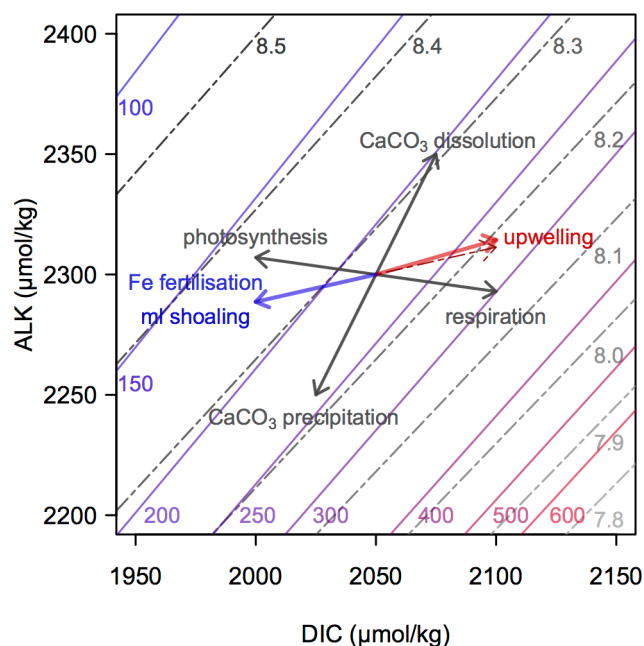
Supplementary Figure 1 Dissolved Inorganic Carbon (DIC) versus Alkalinity (ALK) with contours of pH on the total scale (grey dashed lines) and pCO$_2$ (coloured solid lines) at 5°C, 35 PSU and 0m water depth. The effects of photosynthesis and respiration, as well as the precipitation and dissolution of CaCO$_3$ are indicated by the grey arrows. Formation of organic matter by photosynthesis removes DIC and adds ALK in a ratio of ~7:1. Respiration of organic matter adds DIC and removes ALK in the same ratio. Precipitation of CaCO$_3$ removes both DIC and ALK with a ratio of 1:2 and dissolution of CaCO$_3$ adds DIC and ALK in the same ratio. The effects of an increase in export production from iron fertilisation and mixed layer shoaling are indicated by the blue arrow (assuming a C$_{org}$:CaCO$_3$ rain ratio of 4:1). The effect of an increase in upwelling of subsurface waters containing the respired/dissolved products exported from a surface ocean with a C$_{org}$:CaCO$_3$ rain ratio of 4:1 is shown by the solid red arrow; the effect of upwelling waters from 250m depth into the surface of the modern western subpolar North Pacific using the values from ref[15] is shown by the dashed red arrow. The upwelling of waters from the ocean's interior brings with it the respired products of photosynthesis, increasing the ratio of DIC to alkalinity (ALK), lowering pH and increasing CO$_2$ (red arrow). Increasing export production through the alleviation of iron or light limitation decreases the ratio of DIC/ALK, increasing pH and decreasing CO$_2$ (blue arrow).
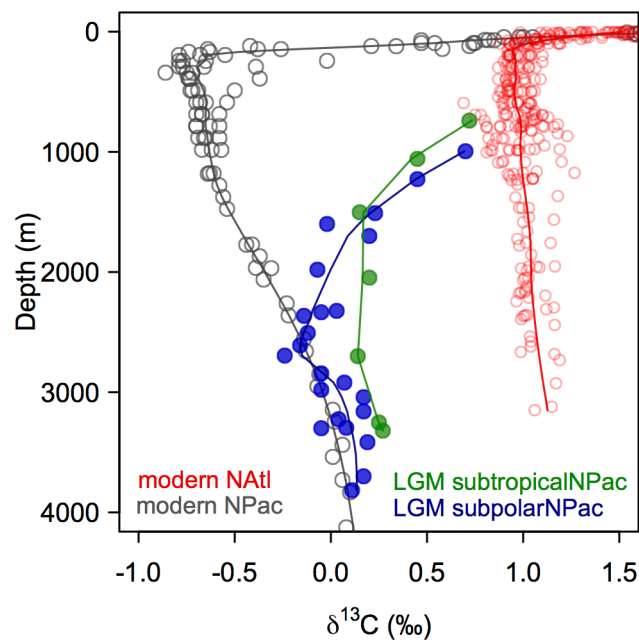
Supplementary Figure 2 δ^{13}C profiles of the modern (grey) and LGM (blue and green) NW Pacific, and modern North Atlantic (red). Modern values are DIC measurements from ref[15]. LGM values are *Cibicidoides* spp. from refs[29,34]. LGM values have been corrected for the whole ocean change in δ^{13}C using ref[87].
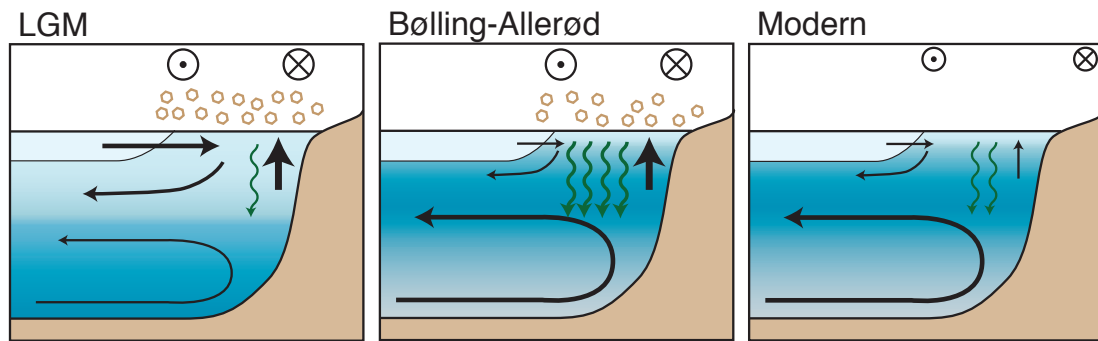
Supplementary Figure 3 Schematic of circulation and upwelling (black arrows), productivity (green arrows) and atmospheric iron supply (brown symbols) during the LGM, Bølling-Allerød, and in the modern North Pacific. At the LGM, ice sheets on North America shift the easterlies south and strengthen the westerlies, driving increased Ekman suction. However, the upwelled waters have relatively low nutrient contents, due to enhanced ventilation of the upper water column by NPIW, analogous to a shallower version of the modern North Atlantic. During the Bølling-Allerød warming NPIW collapses, increasing the nutrient content of subsurface waters. The continued presence of ice on North America maintains high Ekman upwelling, driving a high flux of nutrients and CO_2 into the surface. Relatively high iron availability from dust, along with reduced light limitation due to seasonal stratification, also contribute to high export productivity, but are not its primary cause. The linked combination of reduced ventilation and high productivity drives hypoxia at intermediate depths.

Supplementary Figure 4 New age model used in this study (purple), and previously published plateau-tuned age model of ref[47].
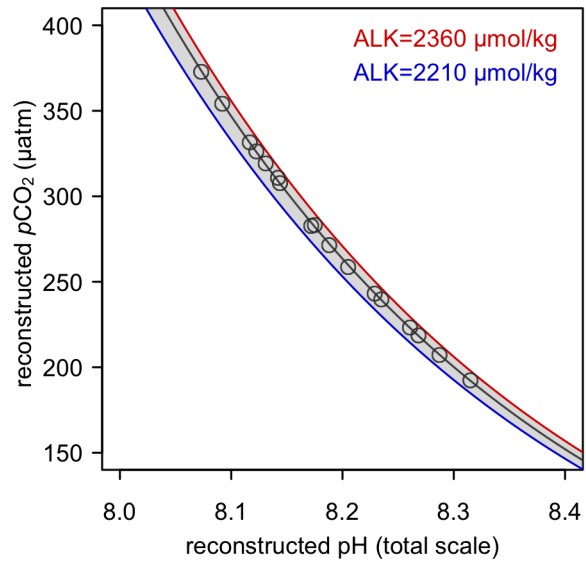
Supplementary Figure 5 Reconstructed pCO$_2$ as a function of reconstructed pH with varying alkalinity. The range in alkalinity represented by the shaded area is equivalent to the range in alkalinity found within the surface of the open Pacific Ocean today[15].
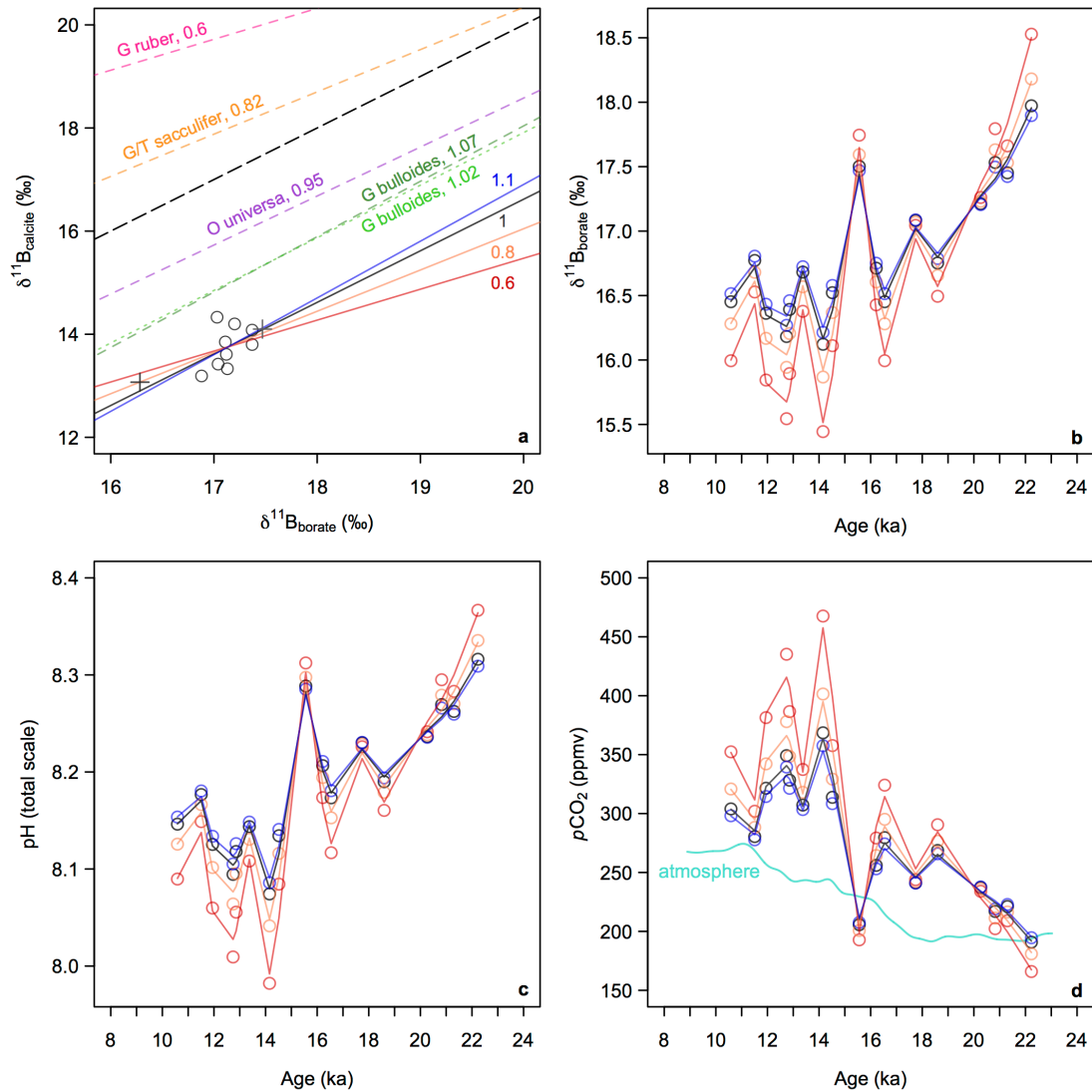
Supplementary Figure 6 $\delta^{11}B_{calcite}$-$\delta^{11}B_{borate}$ calibration sensitivity test **(a)** the dashed lines show all previously published planktic foraminiferal relationships between $\delta^{11}B_{borate}$ and $\delta^{11}B_{calcite}$ (refs[18,65,66]) with the slope of the relationship indicated. The 1:1 line is shown by the dashed black line. *N. pachyderma* coretop data of ref[65] are shown by the open circles. To test the sensitivity of our results to the assumed slope of the calibration line we re-calibrated the coretop data of ref[65], forcing the slope of the line within the range previously observed in all other species of planktic foraminifera (0.6 to 1.1, solid lines), and allowing the intercept to vary. Newly generated Holocene $\delta^{11}B_{Npachyderma}$ from MD01-2416 (dark-grey cross) and MD02-2489 (light-grey cross; 54.39°N, 148.92°E, 3640 m water depth) plotted against pre-industrial $\delta^{11}B_{borate}$, show very good agreement with the calibration proposed by ref[65] used in this study **(b)** down core $\delta^{11}B_{borate}$ **(c)** pH and **(d)** pCO$_2$ versus age (with LOESS smooth), assuming different slopes in relationship between $\delta^{11}B_{calcite}$ and $\delta^{11}B_{borate}$ (see panel a). This exercise demonstrates that within the range in slope previously observed in all other species of planktic foraminifera, the assumed slope of the $\delta^{11}B_{calcite}$-$\delta^{11}B_{borate}$ calibration makes no difference to any of the conclusions drawn in this study.
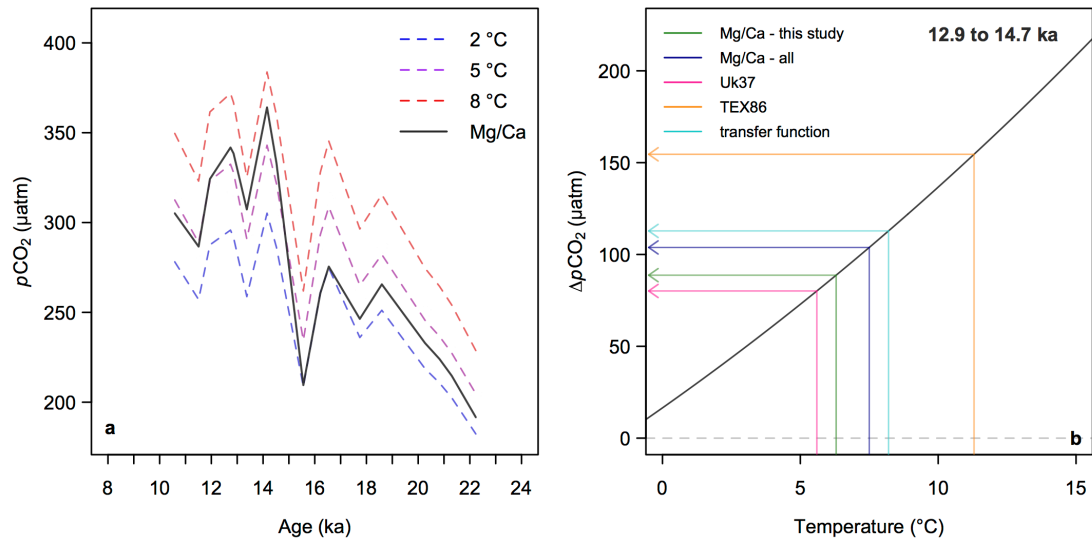
Supplementary Figure 7 Temperature-carbonate system sensitivity tests **(a)** reconstructed pCO_2 versus age at different temperatures (calculated at a constant salinity [33.9] and pressure [5 bar]). The coloured lines are calculated assuming a constant temperature of 2 °C, 5 °C and 8 °C, and the black line shows pH calculated using the Mg/Ca temperatures **(b)** average reconstructed ocean-atmosphere pCO_2 difference (ΔpCO_2) during the Bølling-Allerød (12.9 to 14.7 ka) as a function of temperature (using a salinity of 33.9 and pressure of 5 bar). Coloured lines show reconstructed temperature within the western subpolar North Pacific during this interval from all available proxy data (refs[21,80-82]). The temperatures suggested by all proxies suggest a substantial outgassing of CO_2 to the atmosphere during the Bølling-Allerød.
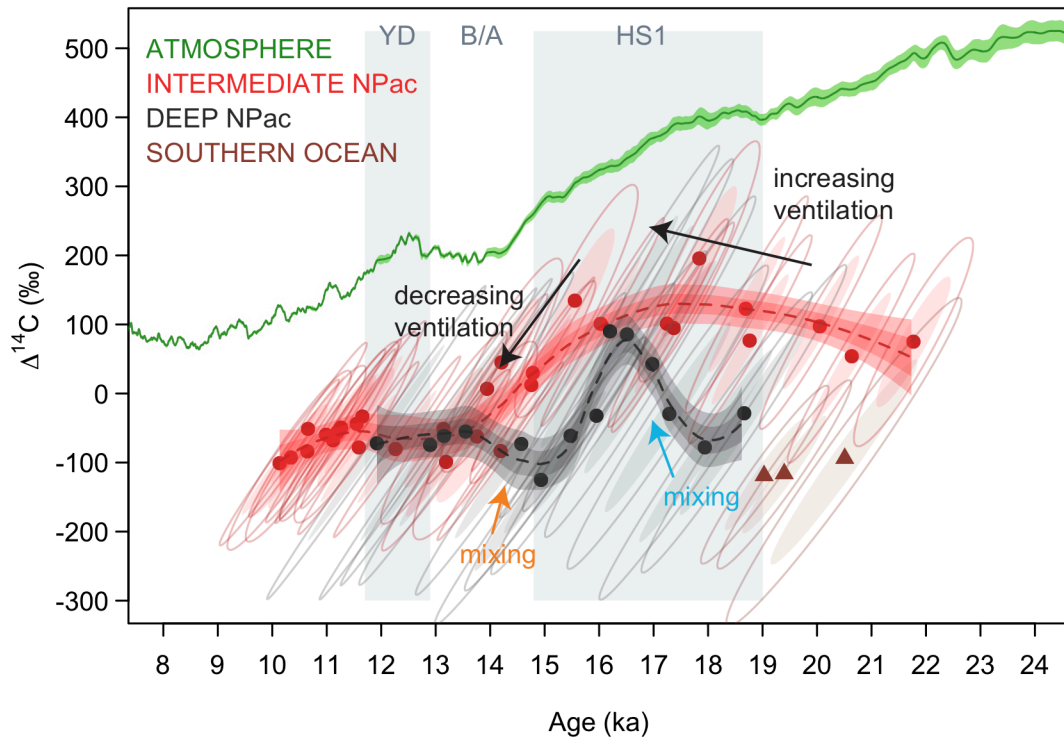
Supplementary Figure 8 Benthic Δ^{14}C records from the intermediate (<1500m) western North Pacific[30] (red circles, see caption of Figure 3 for core details) and deep North Pacific[35,47] (black circles), with the atmospheric record of ref[48] (green), and the LGM Southern Ocean data of ref[S1] (brown triangles). Confidence intervals are 95% (open circles) and 67% (filled circles). LOESS smooth shown by the dashed line with 67% and 95% confidence intervals. An increase in North Pacific overturning circulation is suggested during early deglaciation by increasing Δ^{14}C, with deepwater formation in HS1 resulting in mixing throughout the water column to ~3600m (blue arrow). A reduction in intermediate water formation during the Bølling-Allerød results in old, radiocarbon depleted, deepwaters mixing throughout the water column, and low Δ^{14}C values at intermediate depths (orange arrow). The Southern Ocean record of ref[S1] is thought to represent southern sourced deepwater, which flows into the deep Pacific today, and likely during the LGM.
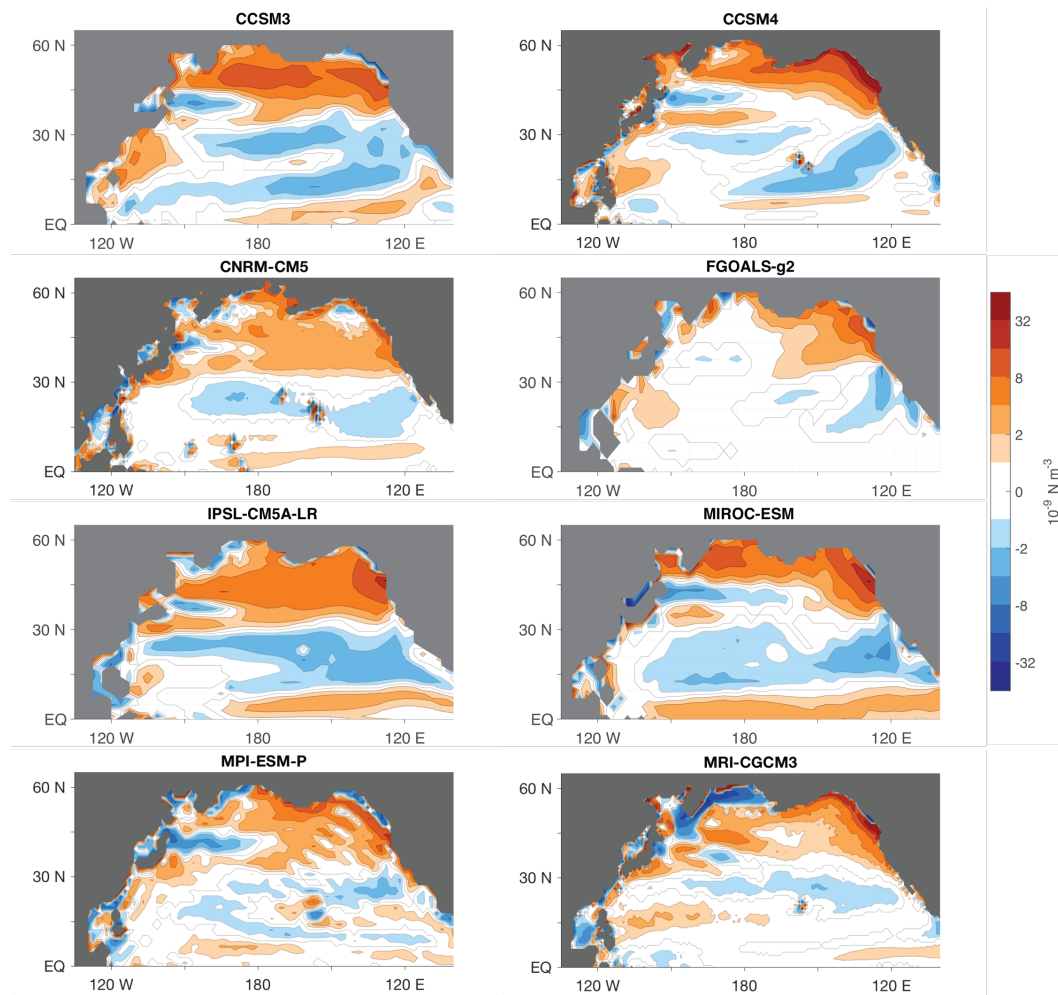
Supplementary Figure 9 Difference in wind stress curl within the North Pacific under glacial boundary conditions relative to pre-industrial control in PMIP3 climate model ensemble[31].

Supplementary Table 1

The location of cores in the North Pacific from which proxy data are discussed in the manuscript

Core	Lat (°N)	Lon (°E)	Water depth (m)
RAMA-PC-44	53.00	164.65	2980
PC13	49.72	168.31	2393
ODP882	50.37	167.60	3244
SO202-07-6	51.30	167.70	2345
EW0408-85JC	59.55	-144.15	682
ODP887	54.62	-148.75	3647
ODP1017	34.53	-121.10	955
SO201-2-85KL	57.51	170.70	968
SO178-13-6	52.73	144.71	713
CH84-14	41.73	142.55	978
GH02-1030	42.23	144.21	1212
MR01K03-PC4/PC5	41.12	142.40	1366

Supplementary References

S1.   Skinner, L., Fallon, S., Waelbroeck, C., Michel, E. & Barker, S. Ventilation of the Deep Southern Ocean and Deglacial CO2 Rise. *Science* **328,** 1147–1151 (2010).